Available online at www.sciencedirect.com
ScienceDirect
Journal of Sound and Vibration 302 (2007) 683–698
JOURNAL OF SOUND AND VIBRATION
www.elsevier.com/locate/jsvi

Distributed model for electromechanical interaction in rotordynamics of cage rotor electrical machines

Antti Laiho[a,*], Timo P. Holopainen[b], Paul Klinge[a], Antero Arkkio[c]

[a]*VTT Industrial Systems, P.O. Box 13022, FIN-02044 VTT Espoo, Finland*
[b]*ABB Electrical Machines, P.O. Box 186, FIN-00381 Helsinki, Finland*
[c]*Laboratory of Electromechanics, Helsinki University of Technology, P.O. Box 3000, FIN-02015 HUT Espoo, Finland*

Received 19 September 2005; received in revised form 6 November 2006; accepted 14 November 2006
Available online 2 February 2007

Abstract

In this work the effects of the electromechanical interaction on rotordynamics and vibration characteristics of cage rotor electrical machines were considered. An eccentric rotor motion distorts the electromagnetic field in the air-gap between the stator and rotor inducing a total force, the unbalanced magnetic pull, exerted on the rotor. In this paper a low-order parametric model for the unbalanced magnetic pull is coupled with a three-dimensional finite element structural model of the electrical machine. The main contribution of the work is to present a computationally efficient electromechanical model for vibration analysis of cage rotor machines. In this model, the interaction between the mechanical and electromagnetic systems is distributed over the air gap of the machine. This enables the inclusion of rotor and stator deflections into the analysis and, thus, yields more realistic prediction for the effects of electromechanical interaction. The model was tested by implementing it for two electrical machines with nominal speeds close to one of the rotor bending critical speeds. Rated machine data was used in order to predict the effects of the electromechanical interaction on vibration characteristics of the example machines.

1. Introduction

In an electrical machine the eccentric motion of the rotor distorts the air-gap flux between the stator and rotor inducing unbalanced magnetic pull (UMP) exerted on the rotor. In a machine with nominal speed close to a rotor bending critical speed the UMP may couple the mechanical and electromagnetic system changing the vibrational characteristics of the rotor. The UMP decreases the natural frequencies and may affect the stability of the system by electromagnetic damping induced by the rotor cage currents.

Freise et al. [1] presented the analytical equations for the UMP induced by the eccentric rotor motion. Further, they presented a simple formula to determine the first flexural critical speed starting from the negative spring coefficient induced by the electromagnetic fields. Früchtenicht et al. [2] derived the equations for the UMP when the rotor is in circular whirling motion with arbitrary whirling frequency. Using this model they

*Corresponding author.
E-mail addresses: Antti.Laiho@vtt.fi (A. Laiho), Timo.Holopainen@fi.abb.com (T.P. Holopainen), Paul.Klinge@vtt.fi (P. Klinge), Antero.Arkkio@hut.fi (A. Arkkio).

0022-460X/$ - see front matter © 2007 Elsevier Ltd. All rights reserved.
doi:10.1016/j.jsv.2006.11.032

determined the additional stiffness and damping coefficients induced by the electromagnetic field, and developed an electromechanical (EM) model to study the effects on the rotordynamic stability. Belmans et al. [3] extended the approach to the two-pole flexible-shaft machines including the effect of the unipolar flux.

Arkkio et al. [4] presented a low-order parametric model for the forces between the stator and rotor. Holopainen et al. [5] extended the model by introducing cage current variables modeling the rotor cage currents. Furthermore, Holopainen et al. [6] combined the force model to Jeffcott rotor model and studied stability of the system.

The effect of UMP on vibrational characteristics of electrical machines has been under active research [7–10]. Ha et al. [11,12] considered transient analysis of a mass unbalanced rotor under UMP. They carried out time stepping procedure by solving the magnetic field equations in the air-gap to obtain UMP exerted on rotor shaft which was modeled by a structural finite element (FE) model. Tenhunen et al. [8] studied the UMP exerted on the cage rotor in conical whirling motion. They applied a numerical calculation model, where the core section was divided into a set of slices perpendicular to the machine axis. The rotor shaft and stator core were assumed to be rigid. The electromagnetic field of individual slices was solved by the FE method and the slices were coupled together by the rotor cage and stator winding currents. They validated the model by test measurements for a 15 kW cage induction motor.

In this paper, we consider the rotor vibrations of cage rotor machines having nominal running speed close to rotor bending critical speed. We present a computationally effective distributed EM interaction model for examining the effect of UMP on rotor system vibrations. A low-order parametric model for UMP [5] was extended and combined to three-dimensional (3D) FE structural analysis model of the mechanical system including the rotor, stator, sleeve bearings, foundation, and machine housing. Owing to the rotor bending modes lying at the low-frequency range the system order reduction was efficiently carried out by modal superposition method. Unbalanced mass response and orbital analysis of the rotor center locus under electromagnetic interaction were considered.

2. Methods

The basis of our research lies on the parametric electromagnetic force model introduced by Holopainen et al. [5]. In this analysis we utilize the sliced structure of the rotor and stator each slice being perpendicular to the rotor shaft. We apply the parametric model on each slice. The separate slices are coupled by the cage current formulation manifesting the continuity condition of the cage currents.

2.1. Electromagnetic force model

Holopainen et al. [5] presented a simple parametric model for the electromagnetic force. This parametric model describes the total force between the rotor and stator in transversal plane. The following main assumptions are used in the derivation of the model: (a) the rotor core is a rigid cylinder, (b) the axes of rotor core and stator bore remain parallel during the eccentric rotor motions, (c) there are no parallel paths [13–15] in the stator winding, and (d) the unipolar flux, which may be associated with the eccentricity, particularly in two-pole machines [3], is neglected. In the complex formulation [5] on the transversal plane the electromagnetic total force $F_{\mathrm{em},r}$ exerted on the rotor is given by

$$F_{\mathrm{em},r} = k_0 p_c + c_- g_- + c_+ g_+, \tag{1}$$

$$\dot{g}_\pm + (\tau_\pm^{-1} + \mathrm{j}\omega_\pm) g_\pm + b_\pm \dot{p}_c + \mathrm{j} b_\pm \omega_\pm \, p_c = 0, \tag{2}$$

where dot refers to the time derivative and $\mathrm{j}^2 = -1$. In Eqs. (1) and (2) the complex variable p_c denotes the transversal displacement of the rotor axis with respect to the center line of the stator bore and $g_\pm$ are referred to as the cage current variables. The subscripts $\pm$ refer to the rotor cage currents of harmonic order $p \pm 1$, the dominant ones in producing UMP, in which p is the number of pole pairs of the machine. In the case $p = 1$ (two-pole machine) only the harmonic component $p + 1$ is present in the formulation with a single cage current variable g_+. The force exerted on the stator is given by $F_{\mathrm{em},s} = -F_{\mathrm{em},r}$.

Table 1
Electromagnetic force model parameters

p	Number of pole pairs
$\tau_\pm$	Time constants of cage currents $p \pm 1$
$b_\pm$	Eccentricity coefficients of cage currents $p \pm 1$
$\omega_\pm$	Relative operational angular frequencies
ω_m, f_m	Rotation frequency
ω_s, f_s	Supply frequency
s	Slip
k_0	Geometric coefficient of eccentricity force
$c_\pm$	Cage current coefficients of eccentricity force
$R_\pm$	Rotor cage resistances of cage currents $p \pm 1$
$L_\pm$	Rotor cage inductances of cage currents $p \pm 1$

In Eq. (2) the rotor cage current time constants $\tau_\pm = L_\pm/R_\pm$ depend on resistances $R_\pm$ and inductances $L_\pm$ of the rotor cage current harmonic components. Furthermore, we have introduced the relative operational angular frequency $\omega_\pm = \pm[\omega_s - \omega_m(p \pm 1)]$ where we have the supply angular frequency $\omega_s = 2\pi f_s$ and the rotor shaft angular frequency $\omega_m = 2\pi f_m$ in which f_s is the supply frequency and f_m the rotational frequency of the rotor. In steady-state operation [5] we have $(1 - s)\omega_s = p\omega_m$ in which s denotes the slip between ω_s and ω_m. Furthermore, under constant flux operation, we have $sf_s = s_{\text{rat}} f_{s,\text{rat}}$ where s_{rat} and $f_{s,\text{rat}}$ are the slip and the supply angular frequency at the rated operational conditions, respectively. Consequently, we obtain $f_s = pf_m + s_{\text{rat}} f_{s,\text{rat}}$ and hence $\omega_\pm = \pm(s_{\text{rat}}\omega_{s,\text{rat}} \mp \omega_m)$.

The relevant electromagnetic parameters are listed in Table 1. The parameters were evaluated at machine rated operation with supply frequency $f_{s,\text{rat}}$ and slip s_{rat} between the fundamental magnetic flux and rotor rotational speed. In Eqs. (1) and (2) the electromagnetic parameters k_0, $c_\pm$, $\tau_\pm$ and $b_\pm$ depend on machine operation conditions, that is, mainly on the rotational speed, supply frequency and load. However, when rotational speed is lower than the rated operation speed the electromagnetic variables can be taken as constants [6]. Above the rated speed, with increasing rotational speed the electromagnetic variables may change considerably. This means that, as we are interested in the rotor bending modes, the analysis is proper for supercritical machines with rated speed higher than the first rotor bending frequency. For subcritical machines the electromagnetic variables have to be evaluated for various rotational speeds since the electromagnetic parameters depend heavily on the operational conditions.

In Eq. (1) the radial part of the force ($k_0 p_c$) represents a well-known negative spring effect in electrical machines. It has been a common practise in industry to include the negative spring effect in FE structural modeling of electrical machines for years. The tangential component of the force is related to the cage current variables $g_\pm$. Tangential force component may bring EM damping to the system or act as a source for instability.

From Eq. (2) we see that the cage current $p \pm 1$ components are fed by the rotor motion with respect to the stator. The attenuation of the cage currents is characterized by the time constant $\tau_\pm$.

The parameters k_0, $c_\pm$ and $b_\pm$ of Eqs. (1) and (2) are numerically estimated by means of the method introduced in Ref. [16]. Indeed, at rated operational conditions, a two-dimensional (2D) coupled field-circuit problem was solved by time-stepping method [17]. As a result, the time-series data for the rotor cage currents and the force exerted on the rotor shaft were obtained. From this data, the current–force frequency responses were calculated by applying Fourier analysis. The parametric model was then fitted to the frequency response data by utilizing least-squares algorithm.

The 3D application of the EM force model presented by Eqs. (1) and (2) is accomplished by slicing the stator core and rotor shaft element models with each slice being perpendicular to the rotor shaft. The rotor shaft is modeled by beam elements and the stator bore is a cylinder around the rotor modeled by solid elements (see Fig. 1(a)). The cage current variables couple the slices manifesting implicit continuity conditions for cage currents.

In the following the FE meshes of the stator core and rotor shaft are supposed to have a sliced structure consisting of N slices perpendicular to the rotor shaft. On each slice $\ell = 1, \ldots, N$ there is a single rotor node

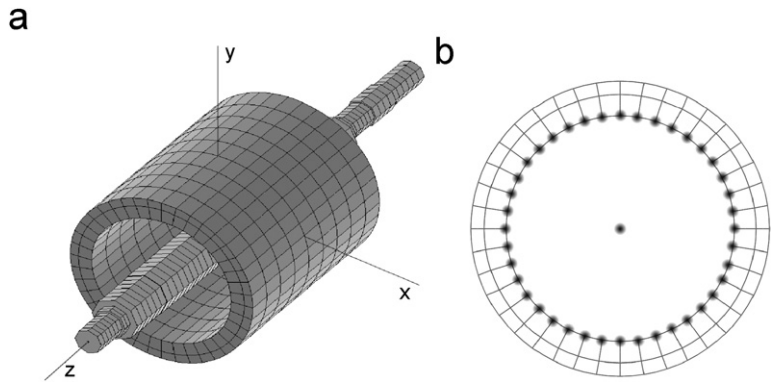

Fig. 1. Slicing the stator and rotor: (a) FE mesh of the stator and rotor and (b) the stator deformation is taken into account by averaging the stator inner core displacements.

with N_ℓ stator bore inner core nodes $\{n_\sigma^\ell\}$, $\sigma = 1, \ldots, N_\ell$ (see Fig. 1(b)). Let us align the z-axis along with the rotor shaft. In order to apply the 2D EM force model given by Eq. (1) we reduce the stator bore inner core node displacements to a single node by averaging procedure. Indeed, the averaged stator bore inner core transverse displacements in x- and y-directions for slice ℓ are given by

$$\hat{u}_{x,s}^\ell = \frac{1}{N_\ell}\sum_{\sigma=1}^{N_\ell} u_x(n_\sigma^\ell),$$

$$\hat{u}_{y,s}^\ell = \frac{1}{N_\ell}\sum_{\sigma=1}^{N_\ell} u_y(n_\sigma^\ell), \tag{3}$$

where $u_x(n_\sigma^\ell)$ and $u_y(n_\sigma^\ell)$ are the x- and y-displacement degrees of freedom (dofs) of the node n_σ^ℓ, respectively.

By applying Eq. (1) we deduce, by slicing in z-direction and including the averaged stator dofs given by Eq. (3), the transversal electromagnetic force exerted on the rotor node of slice ℓ given by

$$F_{\mathrm{em},r}^\ell = \frac{1}{N}[k_0(p_r^\ell - p_s^\ell) + c_- g_- + c_+ g_+], \tag{4}$$

where the complex-valued stator and rotor transversal displacements of slice ℓ are given by $p_s^\ell = \hat{u}_{x,s}^\ell + \mathrm{j}\hat{u}_{y,s}^\ell$ and $p_r^\ell = u_{x,r}^\ell + \mathrm{j}u_{y,r}^\ell$, respectively. By averaging the rotor and stator relative transversal displacements $p_r^\ell - p_s^\ell$ in z-direction over the stator bore we obtain by utilizing Eq. (2) the dynamical equations for cage current variables given by

$$\dot{g}_\pm + a_\pm g_\pm + \frac{b_\pm}{N}\sum_{\ell=1}^{N}(\dot{p}_r^\ell - \dot{p}_s^\ell) + \frac{k_\pm}{N}\sum_{\ell=1}^{N}(p_r^\ell - p_s^\ell) = 0, \tag{5}$$

where we have

$$a_\pm = \tau_\pm^{-1} + \mathrm{j}\omega_\pm,$$

$$k_\pm = \mathrm{j}b_\pm\omega_\pm. \tag{6}$$

If the axis of a rigid rotor remains parallel to the axis of a rigid stator during the eccentric rotor motion, the electromagnetic force model presented by Eqs. (4) and (5) reduces into the form of Eqs. (1) and (2). The form of this reduced parametric model has been numerically verified against more complete FE models [5]. In addition, the experimental validation for this reduced model was carried out by Arkkio et al. [4]. Another special case is the symmetric conical whirling motion studied by Tenhunen et al. [18]. In this motion the center point of the rigid rotor remains fixed but the ends are in whirling motion. In this case, the sums in Eq. (5) become zero and, consequently, the cage current variables $g_\pm$ disappear. This result is compatible with the numerical and experimental results presented by Tenhunen et al. [18]. These observations suggest that the

model presented by Eqs. (4) and (5) can explain the main phenomena related to the cylindrical and conical motion of a rigid rotor presented earlier and it was validated by experimental measurements. However, the deflections of the rotor and stator have been mainly disregarded in previous research.

The EM force and dynamic equations of the slice model given by Eqs. (4) and (5) are written in real matrix form in order to couple them with those of the FE model of the machine. Let us consider the slice ℓ with transversal displacement dofs given by $\mathbf{u}^\ell = (\hat{u}^\ell_{x,s}, \hat{u}^\ell_{y,s}, u^\ell_{x,r}, u^\ell_{y,r})^{\mathrm{T}}$. The electromagnetic force given by Eq. (4) exerted on the stator and rotor nodes of the slice ℓ is written in real vector form as

$$\mathbf{F}^\ell_{\mathrm{em}} = \mathbf{K}^\ell_0 \mathbf{u}^\ell + \mathbf{Q}^\ell \mathbf{g} \tag{7}$$

in which $\mathbf{g} = (g_{-,R}, g_{-,I}, g_{+,R}, g_{+,I})^{\mathrm{T}}$ with R and I denoting the real and imaginary parts, respectively. In Eq. (7) the matrices $\mathbf{K}^\ell_0$ and $\mathbf{Q}^\ell$ are given by

$$\mathbf{K}^\ell_0 = \frac{1}{N}\begin{bmatrix} k_0 & 0 & -k_0 & 0 \\ 0 & k_0 & 0 & -k_0 \\ -k_0 & 0 & k_0 & 0 \\ 0 & -k_0 & 0 & k_0 \end{bmatrix}, \quad \mathbf{Q}^\ell = \frac{1}{N}\begin{bmatrix} -c_{-,R} & c_{-,I} & -c_{+,R} & c_{+,I} \\ -c_{-,I} & -c_{-,R} & -c_{+,I} & -c_{+,R} \\ c_{-,R} & -c_{-,I} & c_{+,R} & -c_{+,I} \\ c_{-,I} & c_{-,R} & c_{+,I} & c_{+,R} \end{bmatrix}.$$

The electromagnetic force exerted on the system composed of the stator and rotor is given by

$$\mathbf{F}_{\mathrm{em}} = \mathbf{K}_0 \mathbf{u}^{\mathrm{sr}} + \mathbf{Q}\mathbf{g}, \tag{8}$$

where $\mathbf{u}^{\mathrm{sr}} = (u^1, \ldots, u^N)^{\mathrm{T}}$ and the matrices $\mathbf{K}_0$ and $\mathbf{Q}$ are obtained by applying matrix building by

$$\mathbf{K}_0 = \begin{bmatrix} \mathbf{K}^1_0 & \mathbf{0} & \mathbf{0} \\ \mathbf{0} & \ddots & \mathbf{0} \\ \mathbf{0} & \mathbf{0} & \mathbf{K}^N_0 \end{bmatrix}, \quad \mathbf{Q} = \begin{bmatrix} \mathbf{Q}^1 \\ \vdots \\ \mathbf{Q}^N \end{bmatrix}.$$

From Eq. (8) we see that $\mathbf{K}_0$ reduces the stiffness of the stator–rotor system while $\mathbf{Q}$ effect on the damping properties.

Dynamics of the cage current variables given by Eq. (5) is formulated in the matrix form as

$$\dot{\mathbf{g}} + \mathbf{K}_c \mathbf{u}^{\mathrm{sr}} + \mathbf{B}\dot{\mathbf{u}}^{\mathrm{sr}} + \mathbf{A}\mathbf{g} = 0. \tag{9}$$

In Eq. (9) we have

$$\mathbf{A} = \begin{bmatrix} a_{-,R} & -a_{-,I} & 0 & 0 \\ a_{-,I} & a_{-,R} & 0 & 0 \\ 0 & 0 & a_{+,R} & -a_{+,I} \\ 0 & 0 & a_{+,I} & a_{+,R} \end{bmatrix},$$

$\mathbf{K}_c = [\mathbf{K}^1_c, \ldots, \mathbf{K}^N_c]$ and $\mathbf{B} = [\mathbf{B}^1, \ldots, \mathbf{B}^N]$ in which we have

$$\mathbf{K}^\ell_c = \frac{1}{N}\begin{bmatrix} -k_{-,R} & k_{-,I} & k_{-,R} & -k_{-,I} \\ -k_{-,I} & -k_{-,R} & k_{-,I} & k_{-,R} \\ -k_{+,R} & k_{+,I} & k_{+,R} & -k_{+,I} \\ -k_{+,I} & -k_{+,R} & k_{+,I} & k_{+,R} \end{bmatrix} \quad \text{and} \quad \mathbf{B}^\ell = \frac{1}{N}\begin{bmatrix} -b_{-,R} & b_{-,I} & b_{-,R} & -b_{-,I} \\ -b_{-,I} & -b_{-,R} & b_{-,I} & b_{-,R} \\ -b_{+,R} & b_{+,I} & b_{+,R} & -b_{+,I} \\ -b_{+,I} & -b_{+,R} & b_{+,I} & b_{+,R} \end{bmatrix}. \tag{10}$$

2.2. Electromechanical interaction model

The equations for the electromagnetic force given by Eqs. (8) and (9) are combined with the equations of motion of the machine. The gyroscopic effect is taken into account by including gyroscopic disks to the model [19]. We utilize structural modal analysis data of the machine. The FE structural analysis is carried out for an

electrical motor and the vibration natural modes and the critical frequencies of the machine are obtained. In the modal regime we obtain

$$\ddot{\boldsymbol{\eta}} + (\mathscr{C} + \boldsymbol{\Phi}^{\mathrm{T}}\mathbf{G}\boldsymbol{\Phi})\dot{\boldsymbol{\eta}} + (\boldsymbol{\Lambda} - \boldsymbol{\Phi}^{\mathrm{T}}\mathbf{K}_0\boldsymbol{\Phi})\boldsymbol{\eta} - \boldsymbol{\Phi}^{\mathrm{T}}\mathbf{Q}\mathbf{g} = \boldsymbol{\Phi}^{\mathrm{T}}\mathbf{F}(t)$$

$$\dot{\mathbf{g}} + \mathbf{K}_c\boldsymbol{\Phi}\boldsymbol{\eta} + \mathbf{B}\boldsymbol{\Phi}\dot{\boldsymbol{\eta}} + \mathbf{A}\mathbf{g} = \mathbf{0}, \tag{11}$$

where we have carried out the system order reduction [20] based on the modal analysis results. In Eq. (11) the displacements $\mathbf{u}$ are given by $\mathbf{u} = \boldsymbol{\Phi}\boldsymbol{\eta}$. The n lowest normal mode shapes including the rotor bending modes form the modal matrix $\boldsymbol{\Phi} = [\phi^{(1)}, \ldots, \phi^{(n)}]$ which is normalized by

$$\boldsymbol{\Phi}^{\mathrm{T}}\mathbf{M}\boldsymbol{\Phi} = \mathbf{I},$$

$$\boldsymbol{\Phi}^{\mathrm{T}}\mathbf{K}\boldsymbol{\Phi} = \boldsymbol{\Lambda} = \boldsymbol{\Omega}_0^2 = \mathrm{diag}(\omega_1^2, \ldots, \omega_n^2),$$

$$\boldsymbol{\Phi}^{\mathrm{T}}\mathbf{C}\boldsymbol{\Phi} = \mathscr{C} = 2\boldsymbol{\Omega}_0\,\mathrm{diag}(\gamma_1, \ldots, \gamma_n), \tag{12}$$

where $\mathbf{I}$ denotes the unit matrix and the diagonal matrix $\boldsymbol{\Lambda} = \boldsymbol{\Omega}_0^2$ is composed of the eigenfrequencies $\omega_1, \ldots, \omega_n$ resulting from the structural FE modal analysis. In Eq. (11) the matrices $\mathbf{M}$, $\mathbf{C}$, $\mathbf{K}$ and $\mathbf{G}$ denote the mass matrix, modal damping matrix, stiffness matrix and gyroscopic matrix, respectively. In Eq. (12) the relative damping coefficients γ_σ are obtained from vibration measurement data of the machine, or, are evaluated by experience.

The state-space formalism of Eq. (11) yields

$$\dot{\boldsymbol{\mu}} + \mathbf{V}\boldsymbol{\mu} = \mathbf{f}(t) \tag{13}$$

in which $\boldsymbol{\mu} = (\dot{\boldsymbol{\eta}}, \boldsymbol{\eta}, \mathbf{g})^{\mathrm{T}}$ and $\mathbf{f}(t) = (\boldsymbol{\Phi}^{\mathrm{T}}\mathbf{F}(t), \mathbf{0}, \mathbf{0})^{\mathrm{T}}$ and the system matrix $\mathbf{V}$ is given by

$$\mathbf{V} = \left[\begin{array}{c|c|c} \mathscr{C} + \boldsymbol{\Phi}^{T}\mathbf{G}\boldsymbol{\Phi} & \boldsymbol{\Lambda} - \boldsymbol{\Phi}^{T}\mathbf{K}_0\boldsymbol{\Phi} & -\boldsymbol{\Phi}^{\mathrm{T}}\mathbf{Q} \\ \hline -\mathbf{I} & \mathbf{0} & \mathbf{0} \\ \hline \mathbf{B}\boldsymbol{\Phi} & \mathbf{K}\boldsymbol{\Phi} & \mathbf{A} \end{array}\right]. \tag{14}$$

The eigenvalue analysis of $\mathbf{V}$ gives $2n+4$ eigenvalues in conjugate pairs $\lambda_{2\sigma} = \lambda_{2\sigma-1}^*$, $\sigma = 1, \ldots, n+2$, with modal matrix $\boldsymbol{\Pi}$ from which the (complex) normal shapes of the machine are given by the matrix $\boldsymbol{\Phi}\boldsymbol{\Pi}(n+1:2n,:)$. The EM eigenfrequencies $\{f_\sigma\}$ and damping ratios $\{\xi_\sigma\}$ are given by $f_\sigma = |\mathrm{Im}(\lambda_\sigma)|/(2\pi)$ and $\xi_\sigma = -\mathrm{Re}(\lambda_\sigma)/|\lambda_\sigma|$. Furthermore, two electromagnetic extra modes which do not exist in the mechanical model are obtained.

2.3. Dynamic response analysis

Rotating mass unbalanced excitation provides reasonable means of studying motor vibration characteristics [21]. We examine electrical motor by exciting it with a rotating mass placed on the rotor shaft center. Indeed, in Eq. (11) we put $\mathbf{F}(t) = \mathrm{Re}(\mathbf{F}_0 \mathrm{e}^{\mathrm{i}\omega_m t})$ with

$$\mathbf{F}_0 = mR\omega_m^2(0, \ldots, 1, -\mathrm{i}, 0, \ldots, 0)^{\mathrm{T}}$$

in which m is the eccentricity mass, R the eccentricity and the non-zero vector components refer to the transversal dofs of the rotor shaft center node. In order to study the stationary orbits of the rotor shaft center under unbalance mass excitation and electromagnetic interaction we substitute a stationary synchronous trial $\boldsymbol{\mu}(t) = \mathbf{X}(\omega)\mathrm{e}^{\mathrm{i}\omega t}$ to Eq. (13) resulting to

$$\mathbf{X}(\omega) = \boldsymbol{\Pi}\,\mathrm{diag}\left(\frac{1}{\lambda_\sigma + \mathrm{i}\omega}\right)\boldsymbol{\Pi}^{-1}(\boldsymbol{\Phi}^{\mathrm{T}}\mathbf{F}_0, \mathbf{0}, \mathbf{0})^{\mathrm{T}},$$

where we have utilized the eigenvalue data for the system matrix $\mathbf{V}$ given by Eq. (14) with modal matrix $\mathbf{\Pi}$ and eigenvalues $\{\lambda_\sigma\}$. The displacements $\mathbf{u}$ are hence given by

$$\mathbf{u}(t) = \mathbf{\Phi}\,\mathrm{Re}(\mathbf{X}_{n+1:2n}(\omega)\mathrm{e}^{\mathrm{i}\omega t})$$

from which we calculate the receptance and phase for the rotor center node dofs. The rotor center node transversal displacements are given by

$$x(t) = \mathrm{Re}(x_0\mathrm{e}^{\mathrm{i}\omega t}), \quad x_0 = [\mathbf{\Phi}\,\mathbf{X}_{n+1:2n}(\omega)]_{x\mathrm{dof}},$$

$$y(t) = \mathrm{Re}(y_0\mathrm{e}^{\mathrm{i}\omega t}), \quad y_0 = [\mathbf{\Phi}\,\mathbf{X}_{n+1:2n}(\omega)]_{y\mathrm{dof}}.$$

The xy-phase lags between the whirling orbit and unbalanced mass position vectors are hence obtained from the argument angles of x_0 and y_0. The rotor undergoes elliptical whirling with rotor center node following an elliptic orbit [19] with semi-minor and semi-major axes given by

$$\frac{|\sin\gamma|}{\sqrt{\lambda_{1,2}}}$$

in which $\gamma = \arg(y_0) - \arg(x_0)$ and $\lambda_{1,2}$ are eigenvalues of the matrix

$$\frac{1}{|x_0||y_0|}\begin{bmatrix} \dfrac{|y_0|}{|x_0|} & -\cos(\gamma) \\ -\cos(\gamma) & \dfrac{|x_0|}{|y_0|} \end{bmatrix}.$$

3. Results

3.1. 7 MW induction motor

The EM interaction model developed here was applied to a 7 MW cage induction motor. The parameters of the machine are given in Table 2. The motor was assumed to be on a rigid foundation. The oil-film stiffness of the journal bearings was modeled with a symmetric 2×2 stiffness matrix obtained from a commercial journal bearing calculation software [22]. The bearing analysis was carried out at rated speed (2980 rev/min). The damping terms induced by the oil film as well as the effect of operation speed on the bearing stiffness matrices were neglected in order to underline the effects of EM interaction.

The 7 MW motor structural FE model consists of 49 762 elements and 112 869 nodes equipped with 6 dofs each. The modal analysis of the motor was carried out by a commercial structural mechanics FE analysis program. The 13 lowest normal modes covering the frequency range from 0 to 90 Hz were included into the EM model given by Eq. (11). The EM coupling was performed on 6 slices.

The parameters of the electromagnetic force model of the 7 MW motor were determined numerically by the method presented in Ref. [16]. The estimated parameters are presented in Table 3. We assumed the constant flux operation mode of the machine. The justification for this approximation and a more accurate analytical model is given in Ref. [5]. Since the motor has two poles ($p = 1$), a single rotor cage current variable g_+ is included into the analysis given by Eqs. (4) and (5).

In Table 4 the 7 MW motor rotor bending and EM mode modal data are presented. Results are calculated at rated speed for the undamped ($\mathscr{C} = 0$ in Eq. (11)) system. Table 4 shows the normal frequencies of the mechanical (f_0) and EM (f) systems, and the electromagnetically induced damping given as the equivalent viscous damping ratios ξ. Frequency reduction is given by $\Delta f = f - f_0$. The EM damping ratios ξ are slightly

Table 2
The main parameters of the example machines

	7 MW motor	21 MVA generator
Number of pole-pairs	1	7
Number of phases	3	3
Inner diameter of stator core (mm)	630	2020
Radial air-gap length (mm)	6.5	11
Connection	star	star
Rated voltage (V)	6000	13800
Rated frequency (Hz)	50	60
Rated speed (rev/min)	2980	514
Rated current (A)	743	893
Rated power	7.0 MW	21.3 MVA
Rated slip	0.00597	0
Rotor mass (kg)	2997	25 400
Bearing span (mm)	2600	3350

The generator is a salient-pole machine and for the air-gap length is given the minimum value.

Table 3
Electromagnetic parameters of 7 MW motor and 21 MVA generator

	7 MW motor	21 MVA generator
k_0	7.29×10^6 N/m	3.79×10^7 N/m
b_-		1.67×10^6 A/m
b_+	19.95×10^4 A/m	1.16×10^5 A/m
τ_-		3.98×10^{-2} s
τ_+	0.32 s	1.02×10^{-2} s
c_-		10 N/A
c_+	10.07 N/A	20 N/A

The parameters were estimated at rated speed (see Table 2).

Table 4
The calculated modal data for the 7 MW motor at rated rotational frequency (49.7 Hz)

Mode	f_0 (Hz)	f (Hz)	Δf (%)	ξ (%)
Rotor bending 1	27.46	26.60	−3.15	−0.01
Rotor bending 2	35.29	34.65	−1.83	−0.01
EM		49.40		1.00

The mechanical damping was neglected and only EM damping was taken into account.

negative for the rotor bending modes, and, consequently, the EM interaction has a slight destabilizing effect on the rotor bending modes. The effect of EM interaction on other modes (in all 13 modes) included into the analysis was minor. The frequency reduction was up to 3.2% (rotor bending mode 1). The damping ratio was 1.0% for the mode induced by the cage current variables. The remaining modes had negligible damping ratios. The normal frequencies and the electromagnetic damping factors of the undamped EM system as function of rotational speed are depicted in Fig. 4. The results depicted in Fig. 4(a) show that the gyroscopic effect has no effect on the rotor bending modes (Fig. 2).

The unbalanced mass frequency-receptance plot is shown in Fig. 3(a) with phase lags in x- and y-directions depicted in Fig. 5. The modal damping ratios of 16% and 4% for the lower and higher rotor bending modes, respectively, were used. For the other modes damping ratio of 1% was applied. The unbalanced mass excitation was located at the rotor shaft center node and the results evaluated on the same node, as well.

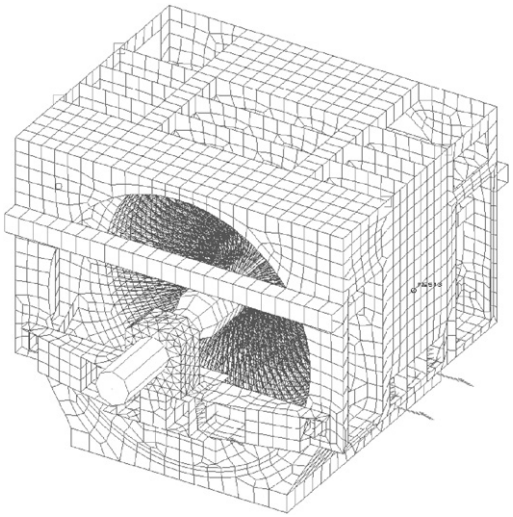

Fig. 2. 21 MVA generator FE model.

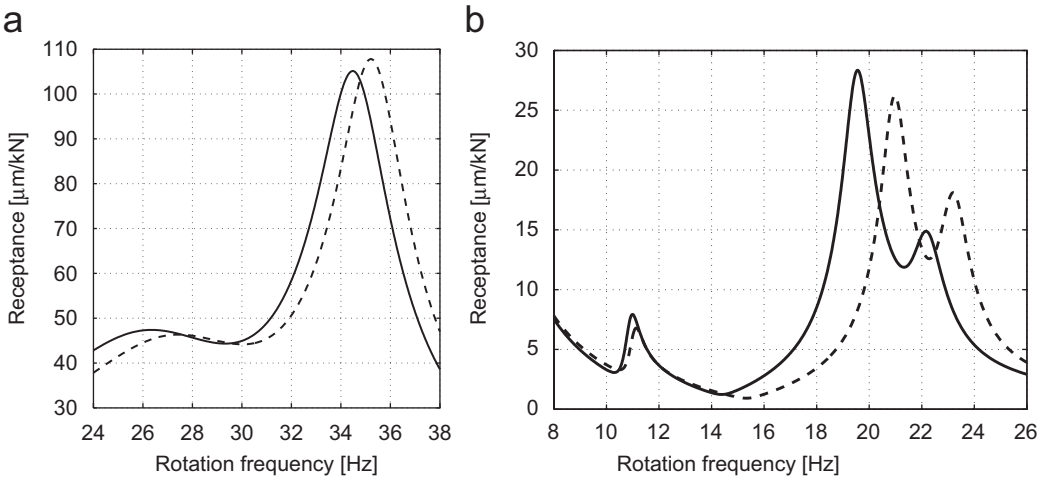

Fig. 3. Unbalanced mass frequency-receptance: (a) 7 MW motor and (b) 21 MVA generator. — Electromechanical system, - - - mechanical system.

The receptance is given as length of the semi-major axis of the rotor center elliptical locus. Due to the positive electromagnetic damping ratios at the vicinity of the second rotor bending mode in Fig. 4(b) the peak receptance of the EM system is slightly lower at the second rotor bending frequency compared to that of the mechanical system (Figs. 3–5).

The eccentricity and orientation of the rotor center elliptical orbit are plotted against excitation frequency in Fig. 6. In Fig. 6(a) the eccentricity ε of the orbit is given by

$$\varepsilon = \sqrt{1 - \left(\frac{b}{a}\right)^2}$$

in which a and b denote semi-major and semi-minor axis length, respectively. In Fig. 6(b) the semi-major axis angle is calculated from positive x-axis showing the transition from the lower to higher rotor bending mode. The eccentricity and orbit angle plots show strong dependence on the rotor bending normal mode shapes which are inclined because of the non-symmetric bearing stiffness in x- and y-directions.

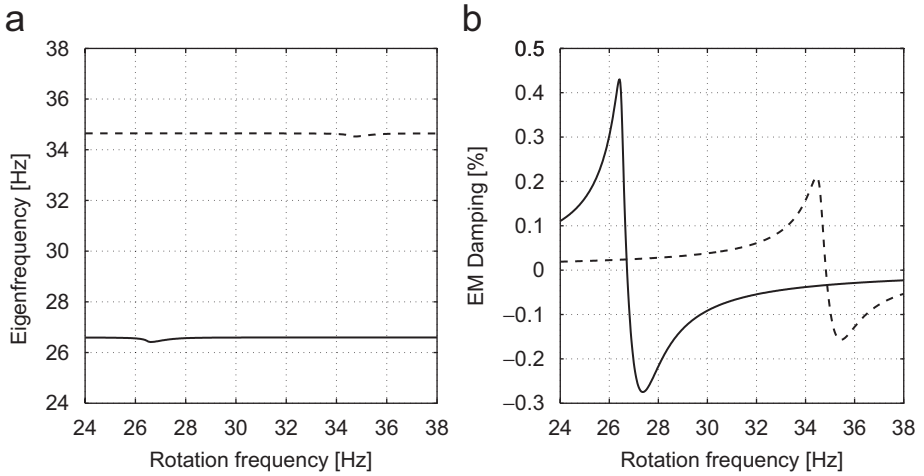

Fig. 4. Eigenanalysis data for 7 MW motor plotted against rotational frequency: (a) eigenvalues and (b) EM damping factors. — Rotor bending mode 1, - - - rotor bending mode 2.

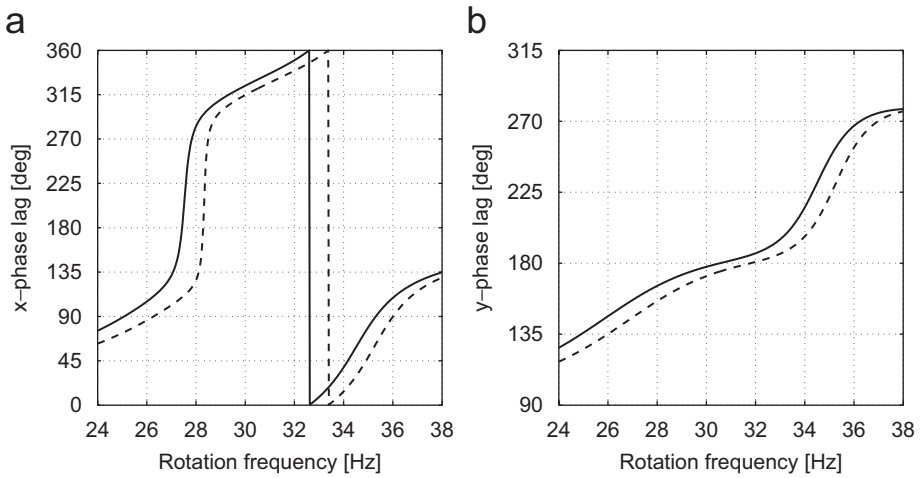

Fig. 5. 7 MW motor rotor center node phase lag between the unbalanced mass and displacement: (a) x-direction and (b) y-direction. — Electromechanical system, - - - mechanical system.

The frequency reduction and receptance versus air-gap length are plotted for lower and higher rotor bending modes in Figs. 7 and 8, respectively. For each air-gap value (20 in total, between $0.3\delta_e$ and $2.0\delta_e$ with $\delta_e = 6.5$ mm from Table 2) the frequency response was calculated for excitation frequency interval 20–28 Hz for lower and 28–36 Hz for higher rotor bending mode. Frequency reduction was determined from the frequency response data of the mechanical and EM systems. The parameter b_+ from Table 3 was varied by $\pm 50\%$. As compared with the single complex dof system given by Eqs. (1) and (2) we obtain from the analytical formulas given by Holopainen et al. [5] that $k_0, c_+ \sim 1/\delta_e$ and from Eq. (2) we find that the frequency reduction is given at the low EM damping (large τ) limit by

$$f_0 - f \approx \frac{k_0 - b_+ c_+}{2\sqrt{km}}. \tag{15}$$

in which m denotes the effective mass and k the effective stiffness of the rotor. The frequency reduction results depicted in Figs. 7(b) and 8(b) for structural analysis framework follow Eq. (15). From the results we see that the parameter b_+ do not have strong influence on the frequency reduction. The receptance versus air-gap

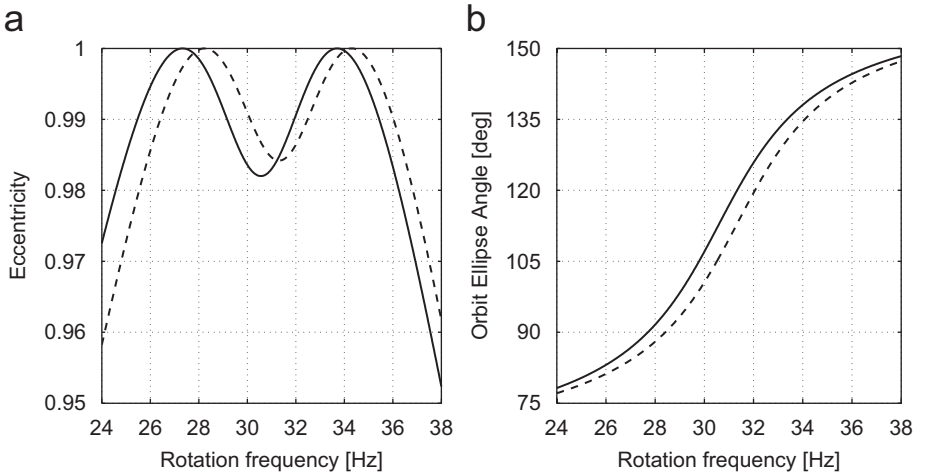

Fig. 6. 7 MW motor rotor center node elliptical orbit data under unbalance mass excitation in rotor center node: (a) eccentricity and (b) semi-major axis angle. — Electromechanical system, - - - mechanical system.

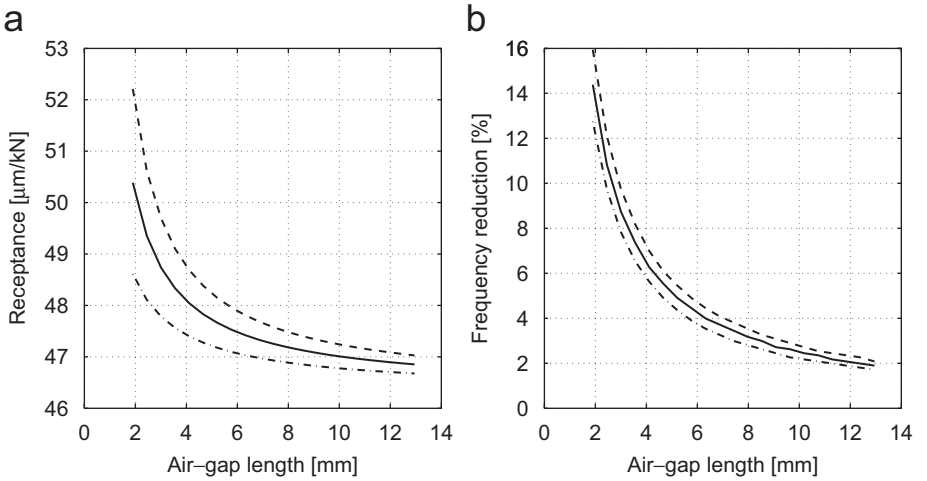

Fig. 7. 7 MW motor rotor bending mode 27.46 Hz: (a) peak receptance and (b) frequency reduction. — b_+, - - - $0.5b_+$, ····· $1.5b_+$.

length is plotted in Figs. 7(a) and 8(a). From Fig. 8(a) we see that receptance at the higher rotor bending frequency gets lower with smaller air-gap when parameter b_+ is large enough.

3.2. 21 MVA synchronous generator

The second numerical example is a 21 MVA synchronous generator. The main parameters of the generator are given in Tables 2 and 3. The parameters $b_\pm$ and $c_\pm$ were evaluated by means of the products $b_\pm c_\pm$ by the approach presented in Ref. [23]. The mounting of the generator was modeled imitating the vibration test conditions carried out for the actual machine. The generator was suspended by elastic springs. The natural frequencies of the suspension system and the machine were below 5 Hz in the numerical model. The FE model mesh of the generator (see Fig. 2) consists of 8905 elements and 9582 nodes with 6 dofs each. The system order reduction was carried out by 30 lowest modes covering the frequency range 0–100 Hz. The EM coupling was implemented by using 13 slices.

The 21 MVA generator modal data calculated from the undamped ($\mathscr{C} = 0$ in Eq. (11)) system at rated speed is presented in Table 5. The normal frequencies f and f_0 are for the EM model and mechanical model,

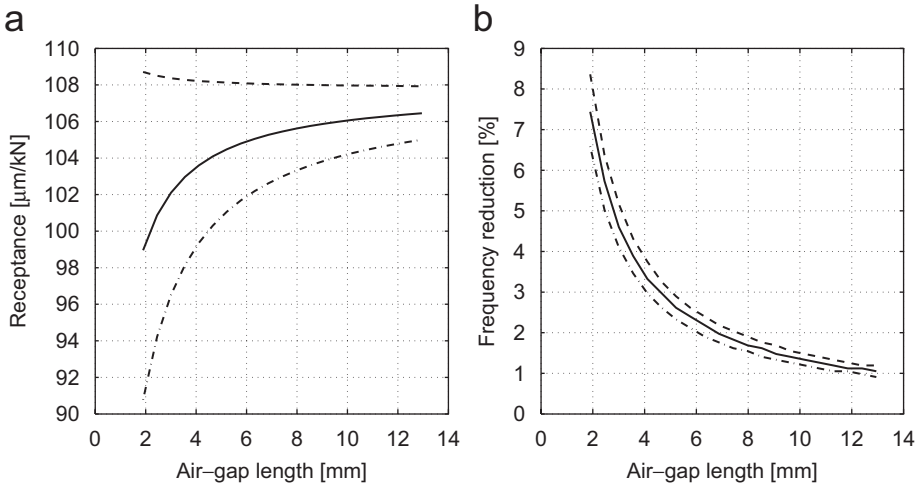

Fig. 8. 7 MW motor rotor bending mode 35.29 Hz: (a) peak receptance and (b) frequency reduction. — b_+, - - - $0.5b_+$, ·---· $1.5b_+$.

Table 5
Modal analysis data of the rotor bending and EM modes of 21 MVA generator at rated rotational frequency (8.6 Hz)

Mode	f_0 (Hz)	f (Hz)	Δf (%)	ξ (%)
EM 1		8.61		87.36
EM 2		8.65		38.91
Bearing block	11.04	10.92	−1.10	0.28
Rotor bending 1	20.85	19.87	−4.70	1.19
Rotor bending 2	23.21	22.43	−3.36	0.73
	41.08	41.06	−0.06	0.01
Conical	43.84	43.72	−0.27	0.00

The mechanical damping was neglected and only EM damping was taken into account.

respectively, with electromagnetic damping ratios ξ. The normal frequencies f_0 of the machine are given by structural FE analysis performed by a structural analysis software package. On contrary to the modal data shown in Table 4 for the 7 MW motor the EM interaction induces damping of the system and therefore has stabilizing effect at rated speed. The two EM modes present in the EM model are well-damped. Again, the effect of EM interaction on other modes (in all 30 modes were included in the analysis) was minor. For them the frequency reduction varied between 0.00% and 0.29% and the damping ratio from −0.000% to −0.005%. The normal frequencies and the electromagnetic damping factors of the undamped EM system as function of rotational speed are depicted in Fig. 9. The results depicted in Fig. 9(a) show that the gyroscopic effect has no effect on the rotor bending modes.

The unbalanced mass frequency response at rotor center node is depicted in Fig. 3(b). A modal damping ratio of 2.5% for rotor bending modes was used based on a separate rotordynamic analysis. For the other modes a damping ratio of 1% was applied. The receptance was calculated as the semi-major axis length of the rotor center elliptical whirling orbit. It must be mentioned that the rated operation speed of this generator is 8.6 Hz. The higher rotation frequencies are presented here in order to show the effects of EM interaction particularly on rotor bending modes.

Effect of the EM interaction on the unbalanced mass response peak amplitudes are characterized by the electromagnetic damping profile given in Fig. 9(b). The rotor bending modes at 20.85 and 23.21 Hz are strongly affected by the EM interaction. At first rotor bending mode frequency (20.85 Hz) the electromagnetic damping term is negative resulting to 8.1% increase in unbalance response (Fig. 3(b)). On the other hand, at second rotor bending frequency (23.21 Hz) the response reduces by 17.8%.

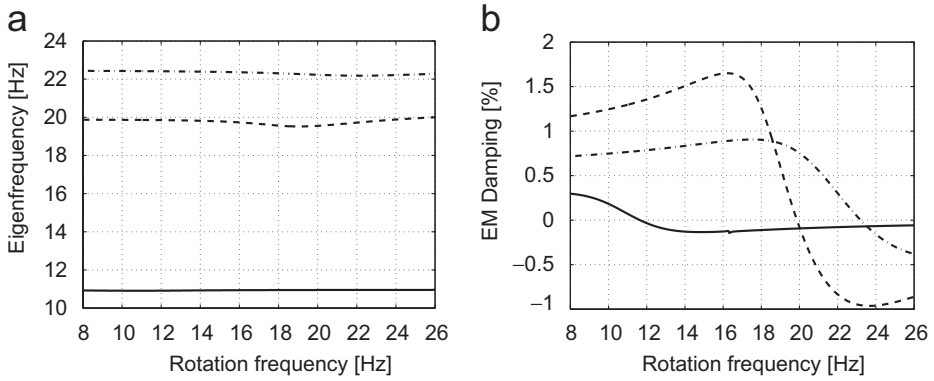

Fig. 9. Eigenanalysis data for 21 MVA generator plotted against rotational frequency: (a) eigenvalues and (b) EM damping factors. — Bearing block mode, - - - rotor bending mode 1, -·-·- rotor bending mode 2.

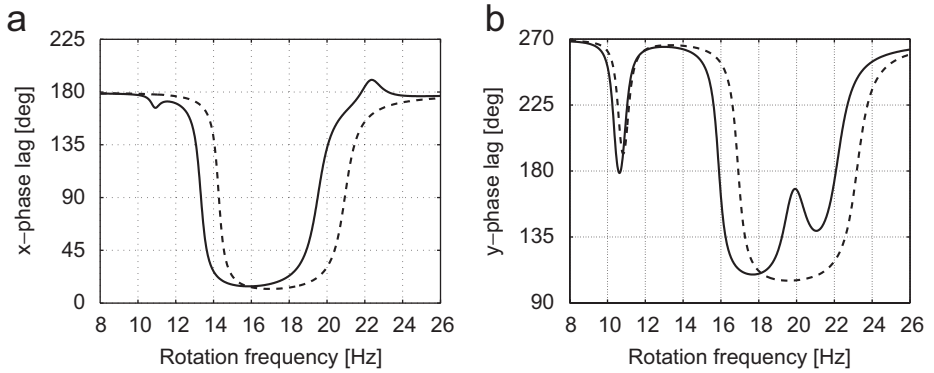

Fig. 10. 21 MVA generator rotor center node phase lag between the unbalanced mass and displacement: (a) x-direction and (b) y-direction. — Electromechanical system, - - - mechanical system.

The x- and y-coordinate phase lags between the rotating mass and rotor position on the elliptical whirling motion are shown in Fig. 10. In Fig. 11 elliptical orbit data is illustrated. The receptance is obtained as semi-major axis length of the orbit ellipse. In addition, the semi-major axis angle with respect to the positive x-axis is depicted.

The frequency reduction and receptance versus air-gap length are plotted for the first rotor bending mode at 20.85 Hz in Figs. 12 and 13. For each air-gap value (20 in total, between $0.3\delta_e$ and $2.0\delta_e$ with $\delta_e = 11.0$ mm from Table 2) the frequency response was calculated for excitation frequency interval 15–21 Hz. The parameters $b_\pm$ from Table 3 were varied in the limits of $\pm 50\%$. Frequency reduction follows Eq. (15). Reduction of the air-gap length strengthens the EM interaction. Furthermore, the electromagnetic damping is negative at the first rotor bending mode frequency in Fig. 9(b). Hence, the reduction of the air-gap length has a destabilizing effect on the first rotor bending mode. The results indicate frequency reduction being dependent on the parameter b_- whereas the dependence on b_+ is minor.

4. Discussion and conclusions

Distortion of the air-gap field induced by eccentric rotor motion couples the mechanical and electromagnetic systems of an electrical machine. In this work the effect of EM coupling on the rotor vibrations of a cage rotor machine was examined. An EM model based on 3D FE structural mechanics modal model combined with a low-order parametric electromagnetic force model was presented. In this model, the interaction between the mechanical and electromagnetic systems is distributed over the air gap of the machine.

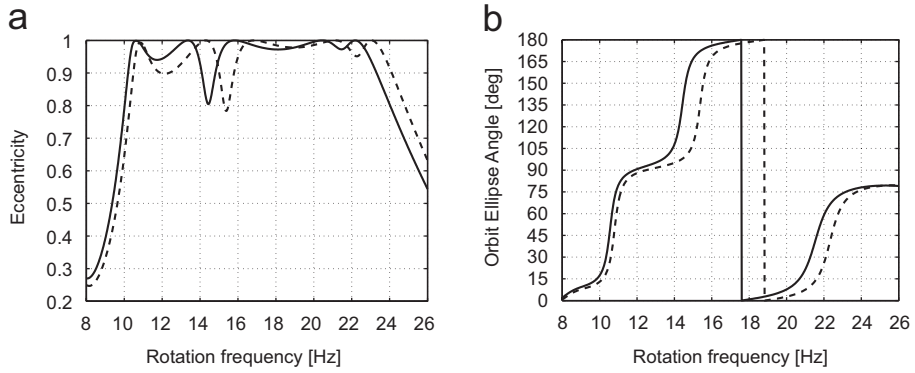

Fig. 11. 21 MVA generator rotor center node elliptical orbit data under unbalance mass excitation in rotor center node: (a) eccentricity and (b) semi-major axis angle. — Electromechanical system, - - - mechanical system.

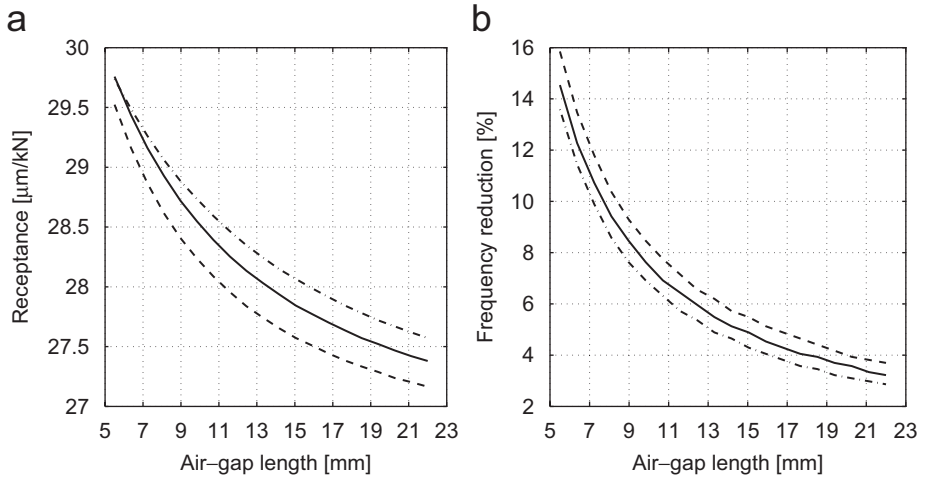

Fig. 12. 21 MVA generator rotor bending mode 20.85 Hz: (a) peak receptance and (b) frequency reduction. — b_-, - - - $0.5b_-$, -·-·- $1.5b_-$.

This enables the inclusion of rotor and stator deformations into the analysis and, thus, yields more realistic prediction for the effects of EM interaction.

The EM model was applied to two test cases, a 7 MW induction motor and 21 MVA synchronous generator. The effects of the EM interaction on the vibrational characteristics of the machines were studied in terms of frequency reduction, EM damping and frequency response analysis. The obtained results confirm the conclusions of previous research that the EM interaction may decrease the natural frequencies of the rotor bending modes, induce additional damping or cause rotordynamic instability. In addition, the developed method enables more refined models to be applied for the rotor and stator and electromagnetic system. This yields enhanced predictive capability to study the EM interaction. The results of these refined models indicate that the effects of EM interaction are apparent on rotor bending modes but minor on other structural modes. The results show that the electromagnetic damping induced by rotor cage currents may have a strong effect on the whirling amplitudes of the rotor bending modes.

In this study, the electrical machines were analyzed without parallel paths in the stator windings. However, in large electrical machines parallel paths are rather the rule than the exception, and likewise, the studied machines include the parallel paths in actual configuration, too. In addition, it is assumed that the parallel paths affect the interaction forces resembling the effects of rotor cage currents by enabling circulatory currents in the stator windings. Secondly, the homopolar flux may have remarkable effects on the vibrations of flexible-shaft two-pole motors [3]. However, in this study, the homopolar flux was ignored in the estimation of EM

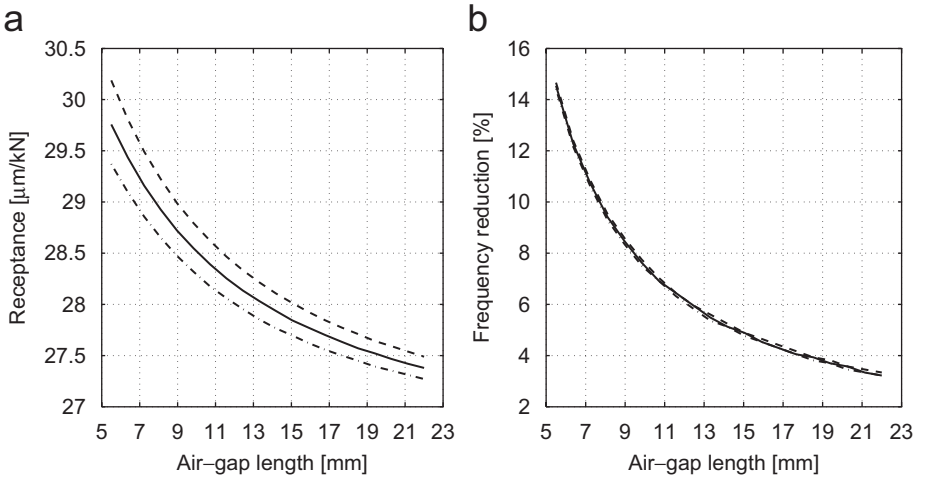

Fig. 13. 21 MVA generator rotor bending mode 20.85 Hz: (a) peak receptance and (b) frequency reduction. — b_+, - - - $0.5b_+$, ----- $1.5b_+$.

force parameters. Furthermore, mechanical damping was modeled as modal damping and damping stemming from the journal bearings was ignored in order to bring out the EM interaction dynamics. However, in practise journal bearings may bring significant damping to the rotor bending modes and therefore suppress the EM interaction. EM interaction model with enhanced bearing modeling needs further consideration and is a matter of future research.

Acknowledgements

The authors are greatly indebted to Mr. Pekka Koskinen, VTT Industrial Systems, for background arrangements. The authors are grateful for Mr. Kari Tammi, VTT Industrial Systems, for valuable suggestions considering the paper. Special thanks are devoted to Mr. Pekka Kanninen and Ms. Päivi Pyysalo, ABB Electrical Machines, for providing the structural finite element models and Mr. Andrejus Burakovas for calculating the electromagnetic force parameters for the 21 MVA generator. The authors gratefully acknowledge the financial support of the Academy of Finland.

References

[1] W. Freise, H. Jordan, Einseitige magnetische zugkräfte in drehstrommaschinen, *ETZ: Elektrotechnische Zeitschrift, Ausgabe A* 83 (1980) 299–303.
[2] J. Früchtenicht, H. Jordan, H.O. Seinsch, Exzentrizitätsfelder als ursache von laufinstabilitäten bei asynchronmaschinen teil, 1 & 2, *Archiv für Electrotechnik* 65 (1982) 217–292.
[3] R. Belmans, A. Vandenput, W. Geysen, Influence of unbalanced magnetic pull on the radial stability of flexible-shaft induction machines, *IEE Proceedings* 134 (2B) (1987) 101–109.
[4] A. Arkkio, M. Antila, K. Pokki, A. Simon, E. Lantto, Electromagnetic force on a whirling cage rotor, *IEE Proceedings—Electric Power Applications* 147 (2000) 353–360.
[5] T.P. Holopainen, A. Tenhunen, E. Lantto, A. Arkkio, Unbalanced magnetic pull induced by arbitrary eccentric motion of cage rotor in transient operation, part 1: analytical model, *Electrical Engineering (Archiv für Electrotechnik)* 88 (1) (2005) 13–24.
[6] T.P. Holopainen, A. Tenhunen, A. Arkkio, Electromechanical interaction in rotordynamics of cage induction motors, *Journal of Sound and Vibration* 284 (3–5) (2005) 733–755.
[7] F.D. Guo, D.C. Chu, The unbalanced magnetic pull and its effects on vibration in a three-phase generator with eccentric rotor, *Journal of Sound and Vibration* 254 (2) (2002) 297–312.
[8] T.-J. Kim, S.-M. Hwang, N.-G. Park, Analysis of vibration for permanent magnet motors considering mechanical and magnetic coupling effects, *IEEE Transactions on Magnetics* 36 (4) (2000) 1346–1350.
[9] T.-J. Kim, S.-M. Hwang, K.-T. Kim, W.-B. Jung, C. Kim, Comparison of dynamic responses for ipm and spm motors by considering mechanical and magnetic coupling, *IEEE Transactions on Magnetics* 37 (4) (2001) 2818–2820.
[10] K.-T. Kim, K.-S. Kim, S.-M. Hwang, K.-T. Kim, Y.-H. Jung, Comparison of dynamic responses for ipm and spm motors by considering mechanical and magnetic coupling, *IEEE Transactions on Magnetics* 37 (5) (2001) 2448–3451.

[11] K.-H. Ha, J.-P. Hong, G.-T. Kim, K.C. Chang, J. Lee, Orbital analysis of rotor due to electromagnetic force for switched reluctance motor, *IEEE Transactions on Magnetics* 36 (4) (2000) 1407–1411.
[12] K.-H. Ha, J.-P. Hong, Dynamic rotor eccentricity analysis by coupling electromagnetic and structural time stepping fem, *IEEE Transactions on Magnetics* 37 (5) (2001) 3452–3455.
[13] D. Dorrell, A. Smith, Calculation of u.m.p in induction motors with series or parallel winding connections, *IEEE Transactions on Energy Conversion* 9 (2) (1994) 304–310.
[14] A. Smith, D. Dorrell, Calculation and measurement of unbalanced magnetic pull in cage induction motors with eccentric rotors. part i: analytical model, *Proceedings of the IEE Electric Power Applications* 143 (3) (1996) 193–201.
[15] D. Dorrell, A. Smith, Calculation and measurement of unbalanced magnetic pull in cage induction motors with eccentric rotors. part ii: experimental investigation, *Proceedings of the IEE Electric Power Applications* 143 (3) (1996) 202–210.
[16] T.P. Holopainen, A. Tenhunen, E. Lantto, A. Arkkio, Unbalanced magnetic pull induced by arbitrary eccentric motion of cage rotor in transient operation, part 2: verification and numerical parameter estimation, *Electrical Engineering (Archiv für Electrotechnik)* 88 (1) (2005) 25–34.
[17] A. Arkkio, Analysis of induction motors based on the numerical solution of the magnetic field and circuit equations, *Acta Polytechnica Scandinavia, Electrical Engineering Series* 59 (1987) 1–97 http://lib.hut/Diss/list.html#1980.
[18] A. Tenhunen, T. Benedetti, T.P. Holopainen, A. Arkkio, Electromagnetic forces of the cage rotor in conical whirling motion, *IEE Proceedings—Electric Power Applications* 150 (5) (2003) 563–568.
[19] R. Garch, R. Nordmann, H. Pfützner, *Rotordynamik*, second ed., Springer, Berlin, 2000.
[20] R.R. Craig Jr., A review of time-domain and frequency-domain component mode synthesis method, *International Journal of Analytical and Experimental Modal Analysis* 2 (2) (1987) 59–72.
[21] J.S. Rao, *Vibratory Condition Monitoring of Machines*, Narosa Publishing House, New Delhi, India, 2000.
[22] SBCALC 3.0, Renk Aktiengesellschaft, Hannover, 2000.
[23] A. Laiho, T. Holopainen, P. Klinge, A. Arkkio, Structural finite element modeling of electromechanical interaction in rotordynamics of electrical machines, *Proceedings of IDETC/CIE*, 2005.